Supporting Information

Activation of actuating hydrogels with WS_2 nanosheets for biomimetic cellular structures and steerable prompt deformation

Lu Zong[†,‡], *Mingjie Li*[†,*], *Jun You*[†], *Xiaochen Wu*[†] *and Chaoxu Li*[†,‡,*]

[†]CAS Key Laboratory of Bio-based materials, Qingdao Institute of Bioenergy and Bioprocess Technology, Chinese Academy of Sciences, Songling Road 189, Qingdao 266101, P. R. China

[‡]University of Chinese Academy of Sciences, 19A Yuquan Road, Beijing 100049, P. R. China

*Corresponding authors: Mingjie Li (Email: limj@qibebt.ac.cn) and Chaoxu Li (Email: licx@qibebt.ac.cn).

Table of contents in Supporting Information:

Supporting figures

Figure S1-Figure S16

Supporting videos

Video S1-Video S12

Supporting figures

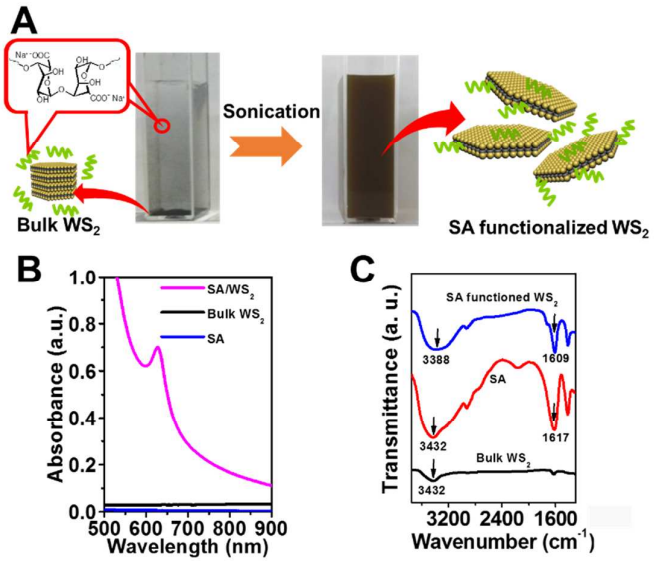

Figure S1. (A) Schematic illustration of alginate-mediated aqueous ultrasonic exfoliation of WS_2 nanosheets. (B) UV−vis absorption spectra of exfoliated WS_2 nanosheets in water. (C) Fourier transform infrared (FTIR) spectra of bulk WS_2, alginate and alginate-exfoliated WS_2 nanosheets. SA: sodium alginate. FTIR spectra were collected using a Thermo Fisher Nicolet 6700 FTIR Spectrometer. UV-vis spectra were taken by a UV-vis-NIR spectrophotometer (PerkinElmer Lambda 25).

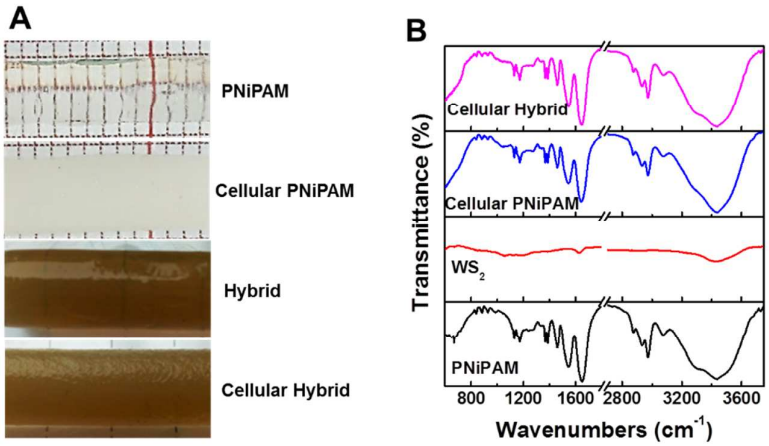

Figure S2. (A) Optical images of as-prepared hydrogels. (B) FTIR of as-prepared hydrogels and WS_2 nanosheets.

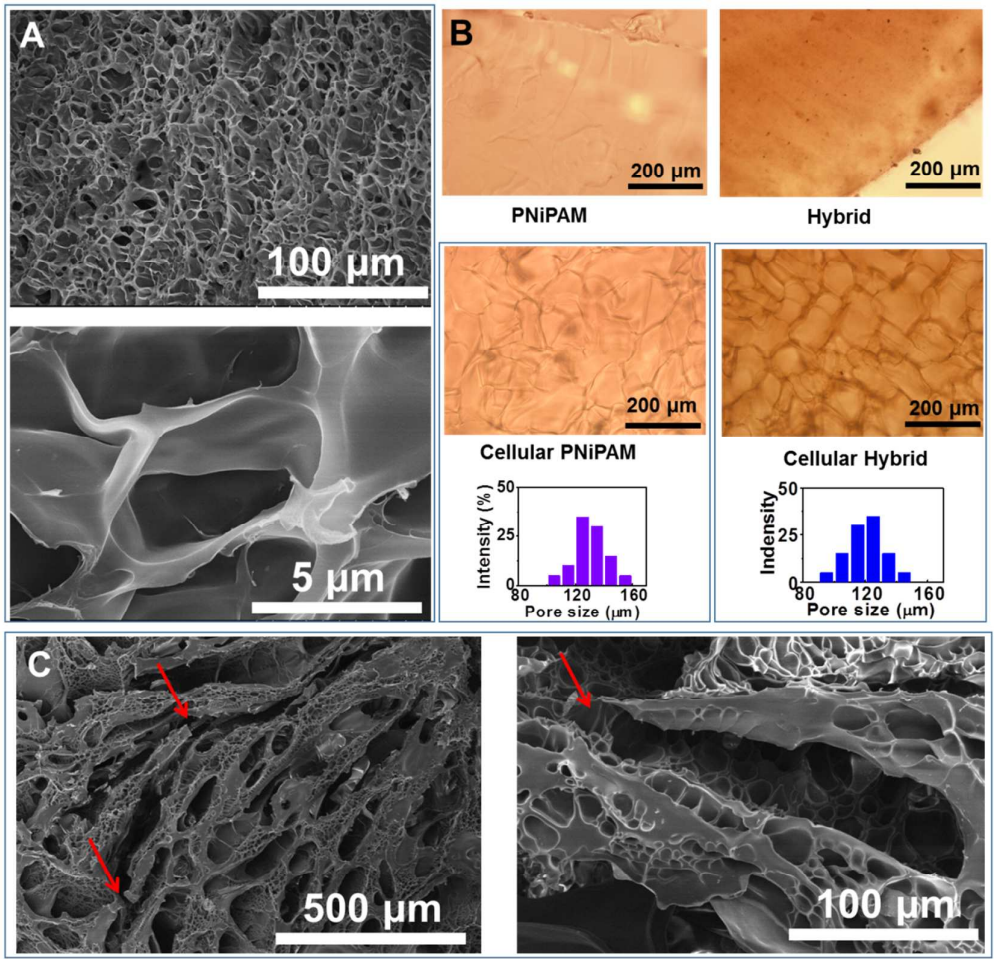

Figure S3. (A) SEM images of freezing-dried *PNiPAM* hydrogel. (B) Optical microscopy images and pore histograms of as-prepared hydrogels. (C) Effect of reverse sequence of freezing and polymerization on microstructures of hybrid hydrogels. The hybrid hydrogel was synthesized by polymerization at 0 °C for 24 h and then freezing at −24 °C for 24 h. Except the reverse sequence of freezing and polymerization, other specific experimental parameters are the same with those for production of *Cellular Hybrid* hydrogel. Apparently, ice-crystallization within the polymerized PNiPAM matrix resulted in inhomogeneous porous structures and local structural fracture.

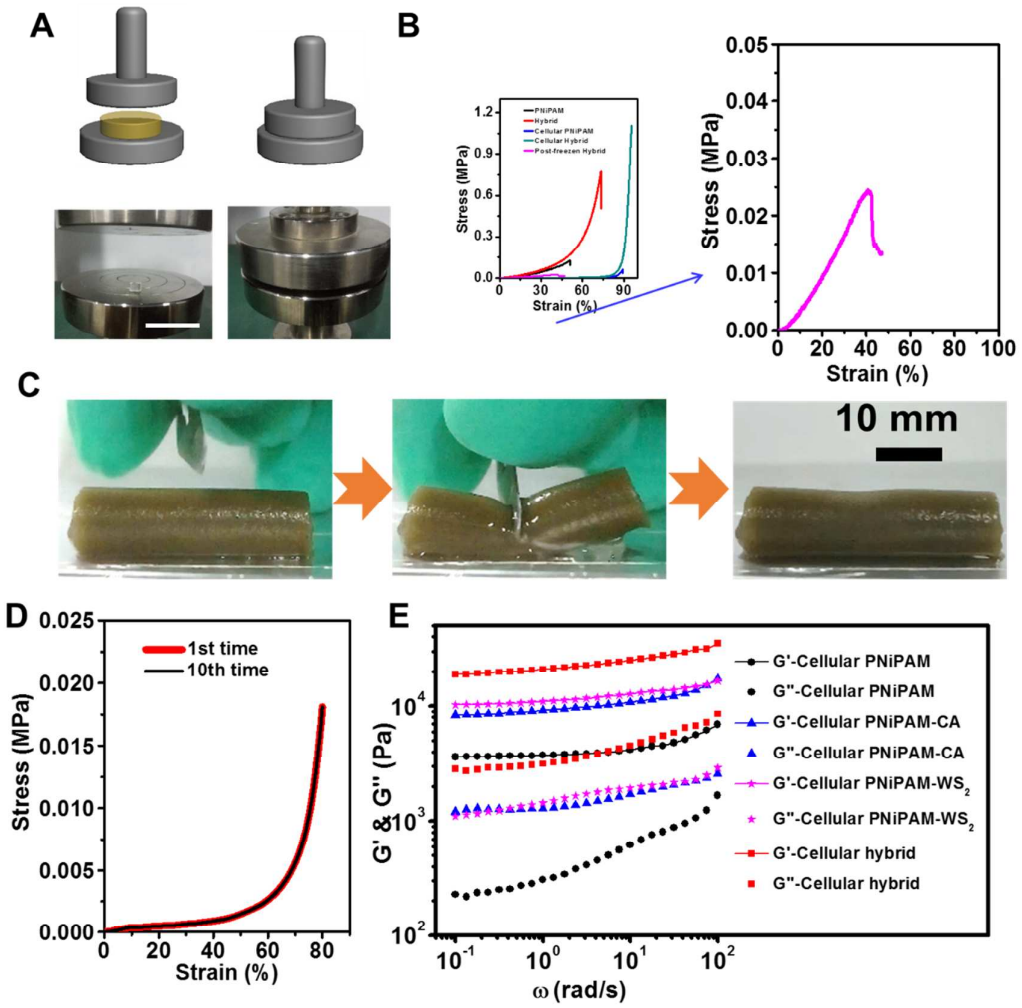

Figure S4. (A) Scheme and optical images showing compression test of cylinder hydrogel. The scale bar is 5 cm. (B) Compression curves of as-prepared hydrogels. *Post-freezen Hybrid* was produced by the reverse sequence of freezing and polymerization (i.e. freezing after polymerization) with with WS_2 nanosheets. (C) Optical images showed that *Cellular Hybrid* hydrogel could withstand sharp scalpel. Scale bar 10 mm. (D) 1st and 10th compression test of *Cellular Hybrid* hydrogel. (E) Mechanical rheological characteristics of as-prepared hydrogels. G′ is storage modulus while G″ refers to loss modulus. *Cellular* PNiPAM, *Cellular* PNiPAM-CA and *Cellular* PNiPAM-WS_2 refer to PNiPAM crosslinked with BIS, BIS + CA and BIS + alginate-modified WS_2, respectively. *Cellular Hybrid* hydrogel displays a dominant elastic solid behavior with G′ > G″, and in spite of the crosslinking from BIS to form solid hydrogel, the contribution from CA crosslinking is much higher

than that of alginate-modified WS_2. Rheological measurements were performed on a MCR 301 rheometer (Anton Paar) equipped with parallel plate grippers of 25 mm in diameter. Oscillatory frequency sweep testing was performed at constant 1% strain (Test temperature: 4 °C).

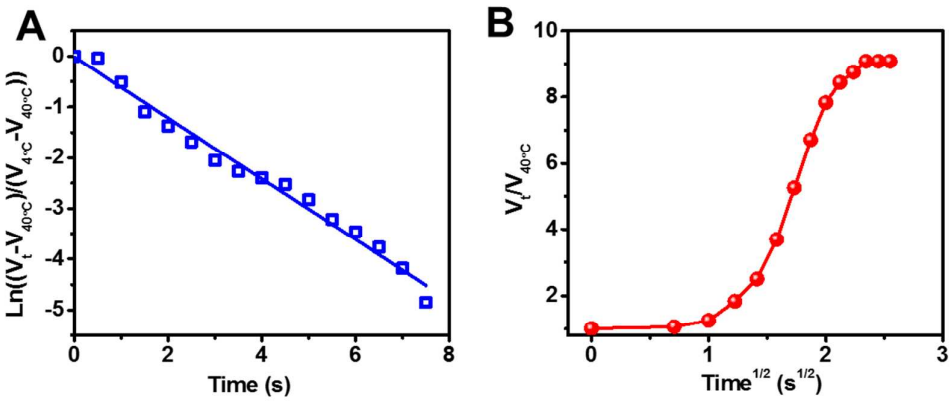

Figure S5. (A) $\ln[(V_t-V_s)/(V_0-V_s)]$ versus time t for shrinkage of *Cellular Hybrid* hydrogel at 40 °C. (B) Swelling kinetics of *Cellular Hybrid* hydrogel at 4 °C. *Cellular Hybrid* hydrogel showed typical sigmoidal patterns indicating that water could permeate within hydrogel easily, thereby endowing fast shrinkage and recovery rates.

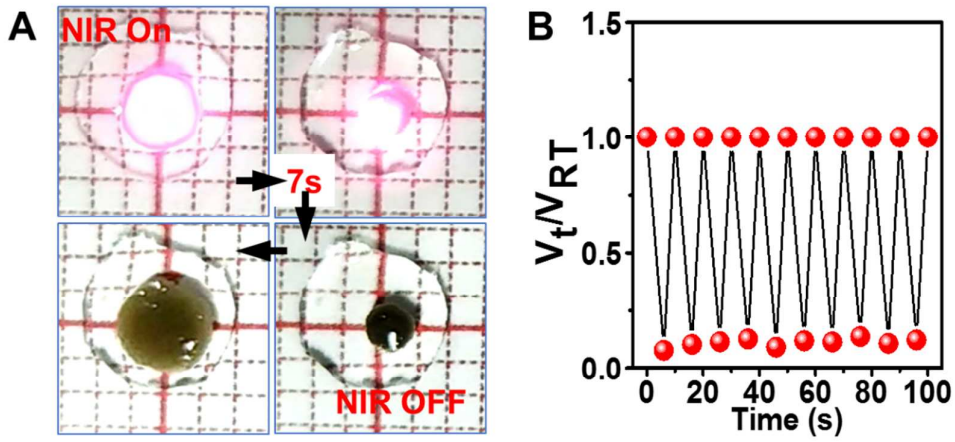

Figure S6. (A) Optical image of shrinkage-recovery cycle of *Cellular Hybrid* hydrogel under NIR radiation (6 W cm^{-2}) at RT. Scale bar of coordinate paper is 2 mm. (B) Repeatability of shrinkage-recovery cycles of *Cellular Hybrid* hydrogel under periodic on-off NIR radiation.

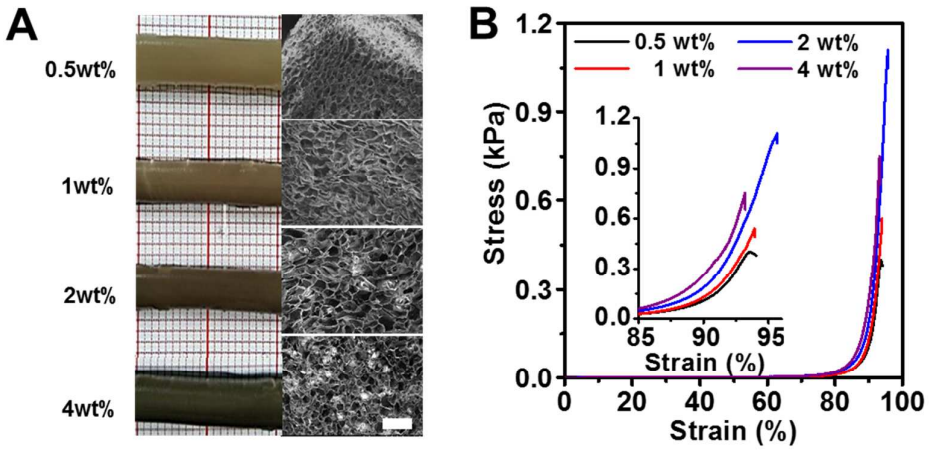

Figure S7. (A) Optical images and corresponding porous microstructures of *Cellular Hybrid* hydrogels with different WS_2 concentrations: 0.5, 1, 2 and 4 wt%. Scale bar of coordinate paper is 2 mm. Scale bar in SEM images is 250 μm. (B) Compression tests of *Cellular Hybrid* hydrogels with different WS_2 concentrations.

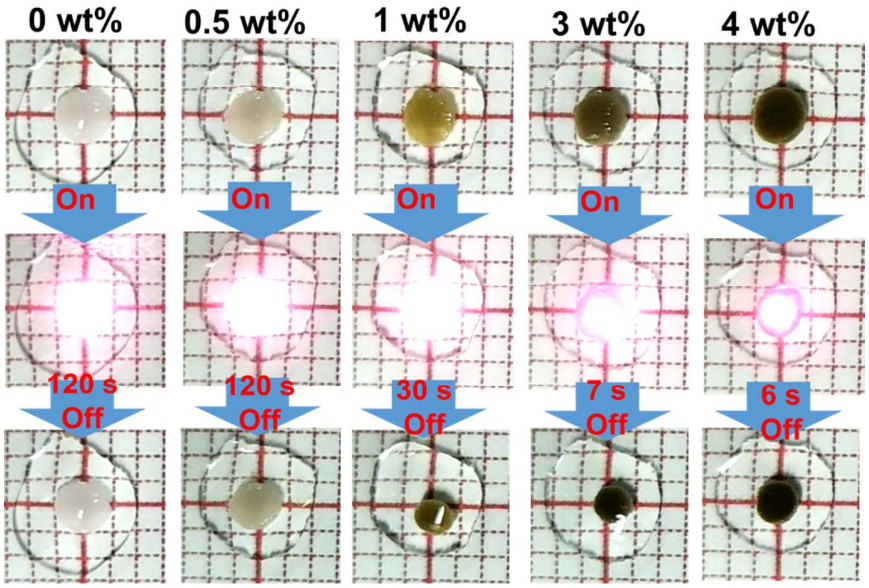

Figure S8. Optical image of shrinking processes of *Cellular Hybrid* hydrogels with different WS_2 concentrations under NIR radiation (6 W cm^{-2}) at RT. Scale bar of coordinate paper is 2 mm.

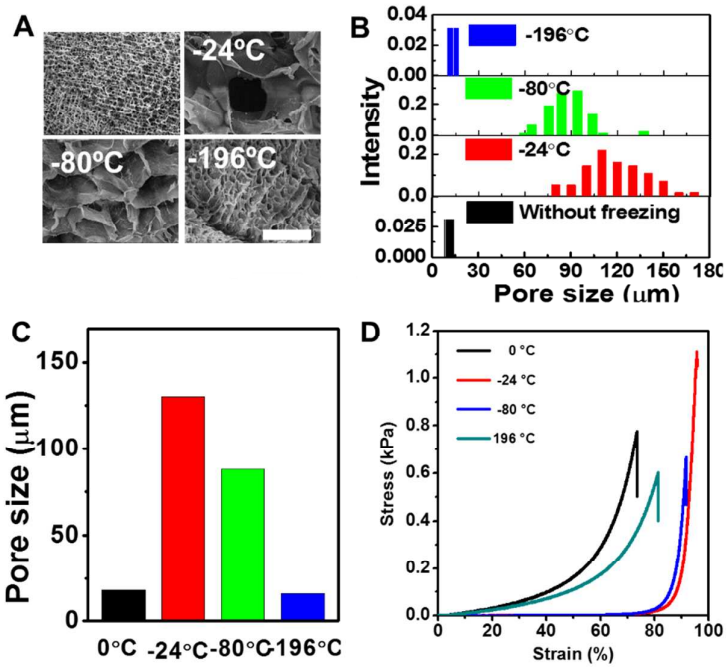

Figure S9. Physical characterization of *Cellular Hybrid* hydrogels prepared at different pre-freezing temperatures: 0, −24, −80 and –196 °C. Scale bar 100 μm. (A) Porous microstructures. (B) Pore histograms. (C) Average pore sizes. (D) Compression tests.

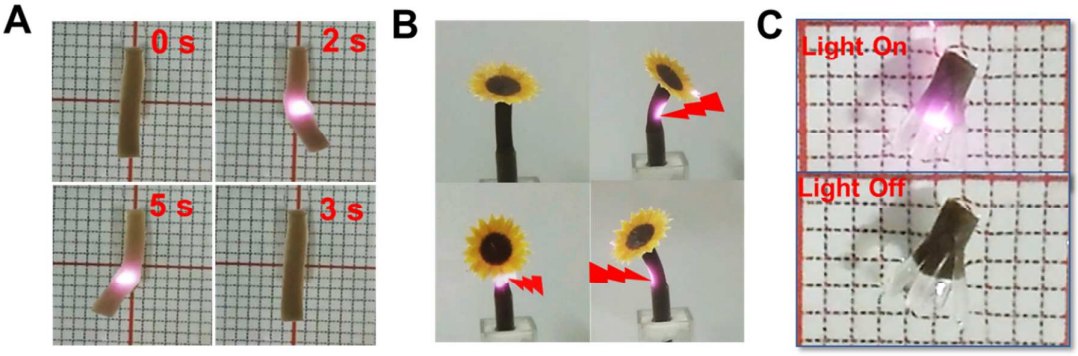

Figure S10. (A) NIR radiation driven actuation behavior of *Cellular Hybrid* hydrogel. Scale bar of coordinate paper is 2 mm. (B) Biomimetic apricus sunflower produced with *Cellular Hybrid* hydrogel. NIR light (0.5 W cm^{-2}). Scale bar 10 mm. (C) Optical images of aquatic swimmer driven by NIR (8 W cm^{-2}). Scale bar of coordinate paper is 2 mm.

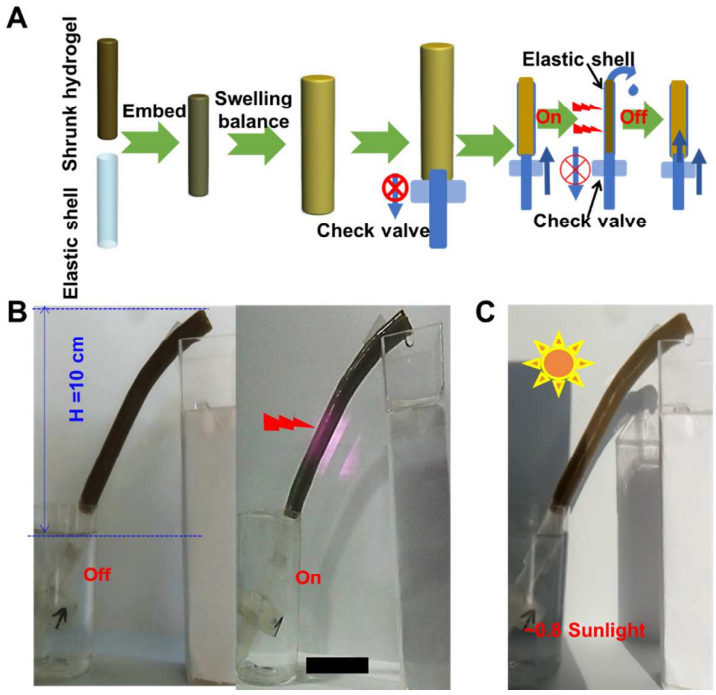

Figure S11. (A) Illustration of construction process of water-lifting filter. (B & C) Optical images of water-lifting process driven by NIR radiation (0.11 W cm^{-2}) (B) and equivalent sunlight light (power density ~ 0.8 sunlight) (C). The scale bar is 20 mm.

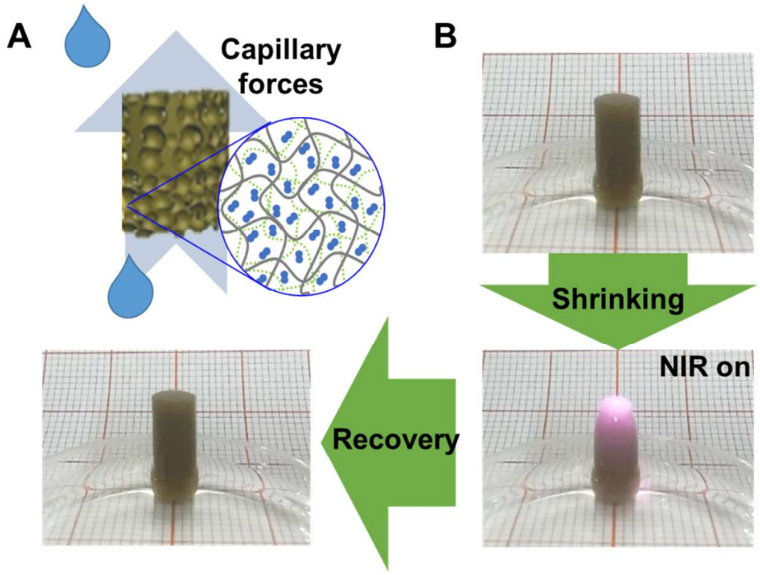

Figure S12. Schematic illustration (A) and optical images (B) of capillary-based water uptake properties of *Cellular Hybrid* hydrogel. Scale bar of coordinate paper is 2 mm.

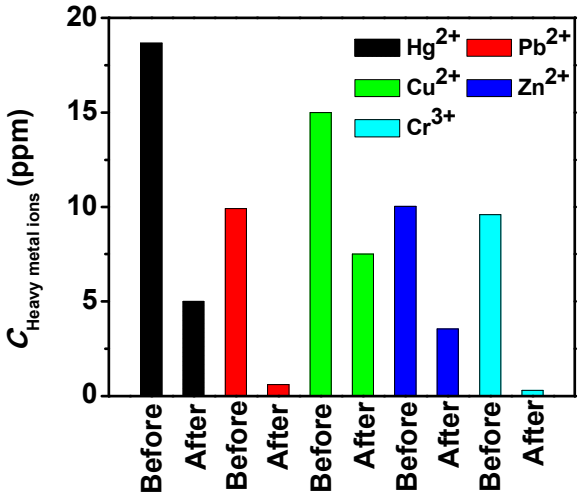

Figure S13. Purification capability of water-lifting filter towards different metal ions.

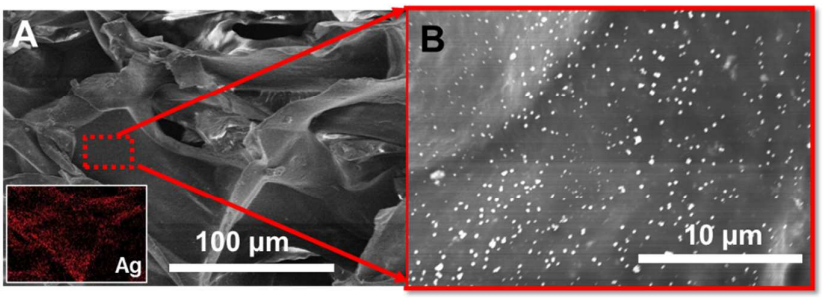

Figure S14. (A & B) SEM images of *Cellular Hybrid* hydrogel embedding with Ag nanoparticles (A) and zoom-in region (B). The inset in (A) is element mapping of Ag.

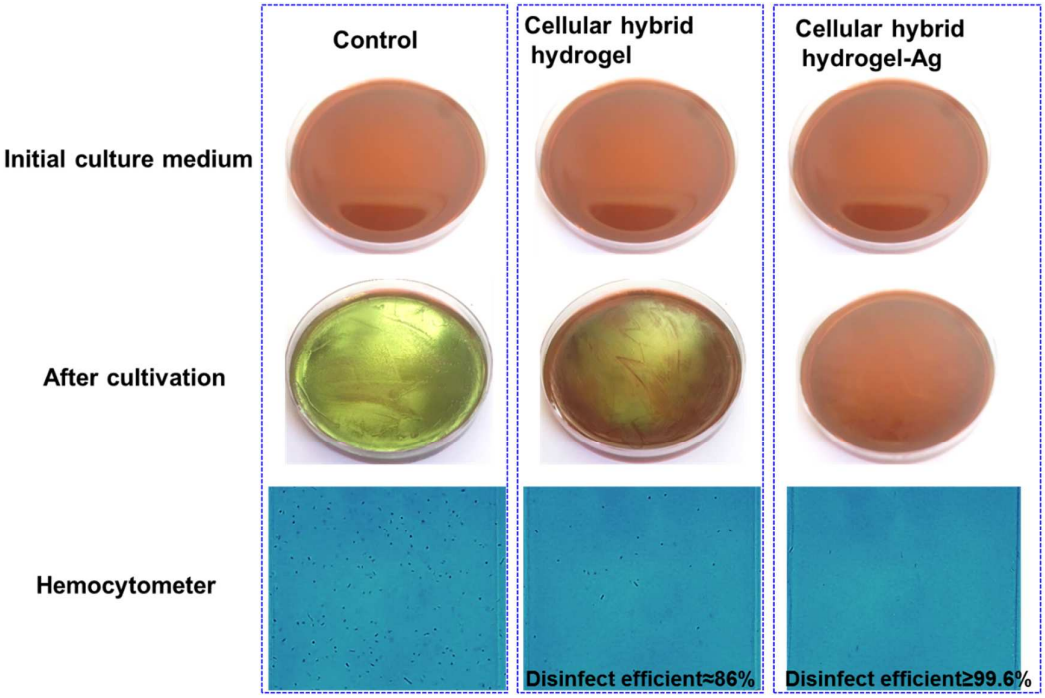

Figure S15. Optical images of eosin-methylene blue medium which was cultured before and after filtered water (containing *E. coli*). Bottom is microphotograph of hemocytometer of re-cultured water containing *E. coli* (diluted times = 100 for a better observed). The disinfect efficiency were also given.

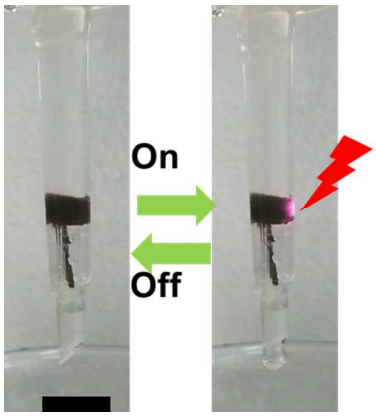

Figure S16. Optical images of light-controlled hydrogel microvalve. Scale bar is 10 mm.

Supporting Videos:

Video S1. Super mechanical properties of *Cellular Hybrid* hydrogel.

Video S2. Rapid volumetric variation of *Cellular Hybrid* hydrogel at 4 °C and 40 °C.

Video S3. Rapid volumetric variation of *Cellular Hybrid* hydrogel exposed to 6 W cm^{-2} NIR radiation and equivalent ~0.8 sunlight at room temperature.

Video S4. Lacking photo-responsiveness of *Cellular PNiPAM* hydrogel under 6 W cm^{-2} NIR radiation.

Video S5. Actuating behavior of *Cellular Hybrid* hydrogel in water under NIR radiation (808 nm, 8 W cm^{-2}) at room temperature.

Video S6. Biomimetic apricus sunflower produced with *Cellular Hybrid* hydrogel under NIR radiation (808 nm, 0.5 W cm^{-2}) at room temperature.

Video S7. Moving aquatic swimmer under NIR radiation (808 nm, 8 W cm^{-2}) at room temperature.

Video S8. Moving rotator on watery surface under NIR radiation (808 nm, 2 W cm^{-2}) at room temperature.

Video S9. Water-liftering behavior of water-lifting filter under NIR radiation (808 nm, 0.11 W cm^{-2}).

Video S10. Capillary driven water-lifting and water release under NIR radiation (808 nm, 0.11 W cm^{-2}).

Video S11. Water-liftering behavior of water-lifting filter under equivalent sunlight (~ 0.8 sunlight).

Video S12. Liquid-microvalve controlled by NIR radiation (808 nm, 1.25 W cm^{-2}).